Desiccation of ecosystem-critical microbialites in the shrinking Great Salt Lake, Utah (USA)

Carie Frantz[1,2]*, Cecilia Gibby[2], Rebekah Nilson[1], Maggie Nguyen[1], Cody Ellsworth[2], Cole J. Stern[1], Hank Dolan[3], Alvin Sihapanya[4], Bonnie K. Baxter[4]

[1] Department of Earth and Environmental Sciences, Weber State University, Ogden, UT, USA

[2] Environmental Science Program, Weber State University, Ogden, UT, USA

[3] Northern Utah Academy for Math, Engineering and Science, Ogden, UT, USA

[4] Great Salt Lake Institute, Westminster College, Salt Lake City, UT, USA

* Corresponding author

E-mail: cariefrantz@weber.edu (CF)

Abstract

Great Salt Lake hosts an ecosystem that is critical to migratory birds and international aquaculture, yet it is currently threatened by falling lake elevation and high lakewater salinity resulting from water diversions in the upstream watershed and the enduring megadrought in the western United States. Microbialite reefs underpin the ecosystem, hosting a surface microbial community that is estimated to contribute 30% of the lake's primary productivity. We monitored exposure, desiccation, and bleaching over time in an area of microbialite reef. During this period, lake elevation fell by 1.8 m, and salinity increased from 11.0% to 19.5% in open-water portions of the outer reef, reaching halite saturation in hydrologically closed regions. When exposed, microbialite bleaching was rapid, driven by a decrease in surface chlorophyll. Bleached microbialites are not necessarily dead, however, with communities persisting beneath microbialite surfaces for several months of exposure and desiccation. However, superficial losses in the mat community resulted in enhanced microbialite weathering. In addition, we conducted microbialite community recovery experiments by incubating bleached microbialite pieces in lakewater and measuring changes in extractable pigments and DNA over time. We observed rapid recovery at salinities ≤ 17%, approaching 50% recovery within 40 days. 16S and 18S rRNA gene sequencing of extracted DNA indicated that recovery was driven by initial seeding from lakewater. At higher salinity levels, recovery occurred more slowly and may reflect accumulation and preservation of lake material in halite crusts vs. true recovery. Our results indicate that increased water input should be prioritized in order to return the lake to an elevation that submerges microbialite reefs and lowers salinity levels. Without quick action to reverse diversions in the watershed, loss of pelagic microbial community members due to sustained high

38 salinity could prevent the recovery of the ecosystem-critical microbialite surface communities in
39 Great Salt Lake.

Introduction

Great Salt Lake: a globally-important ecosystem threatened by water overuse

Great Salt Lake, a terminal lake in northern Utah within the arid Great Basin, is the largest lake in the western United States (Fig 1A). The lake system comprises not only the hypersaline open water but also distinct habitats along a salinity gradient, including fresh- to brackish-water estuaries and wetlands where rivers enter the lake, and expansive mudflats and playas. The main body of the lake is segmented by a rail causeway, which isolates the salt-saturated north arm (Gunnison Bay) from the south arm (Gilbert Bay), which encompasses our study site. The south arm supports a relatively simple but significant food web (Fig 2A); Great Salt Lake is a hemispherically important ecosystem [1] that supports millions of resident and migratory birds [2,3] and a brine shrimp industry that harvests cysts used as feed in global aquaculture [4].

Fig 1. Great Salt Lake field sites and hydrograph. (A) Map of Great Salt Lake showing the north (N) and south (S) arms of the lake with major sites described in this paper: USGS lake elevation sites 1001000 (ES1, Saltair site) and 10010024 (ES2, Causeway site), weather station sites KUTSYRAC22 (WS1) and KUTSYRAC27 (WS2), Buffalo Point microbialite reef sites (BP), and Ladyfinger Point (LFP). Left inset shows the location of Great Salt Lake in northern Utah, USA. Right inset shows the northern tip of Antelope Island. (B) Satellite image of Great Salt Lake from October 29, 2012 and (C) October 28, 2022 showing the shrinking shoreline of Great Salt Lake (MODIS corrected reflectance images from NASA Worldview). (D) Map of Great Salt Lake (at 1280 m elevation) showing the approximate location and extent of submerged vs. exposed microbialite reef areas in summer 2022, after Baskin et al. **[5]**. (E) Lake hydrograph from 1848 to 2022; area highlighted in gray is expanded in (F). The dashed gray line in both figures shows the historical lake lowstand. (G) Detail of field sites at Buffalo Point, with logger sites as vertical bars (B and B3), recovery experiment sites as horizontal bars (RA–RC), and the microbialite monitoring quad with monitored (M1–M3) and cored (C1–C3) microbialites. The 2020 shoreline is also shown as a dashed line. The underlying aerial view (from Google Earth) shows the site in May 2022, with bright areas showing exposed, desiccated microbialites.

Fig 2. Great Salt Lake's microbialite-supported ecosystem. (A) Simplified ecosystem diagram of Great Salt Lake's south arm, illustrating the importance of the lake's microbialites and the effect of microbialite exposure. Dashed arrows represent life cycle stages, solid arrows represent consumption. After Baxter (2018) & Belovsky et al. (2011). (B) Stereo-photomicrograph of a Great Salt Lake microbialite piece imaged at 10x showing a healthy periphyton community, with three-dimensional clumps of *Euhalothece* bound by extracellular polymers, and white points of carbonate highlighted with arrows. Sample collected from Site B on July 7, 2020. (C) Phase contrast photomicrograph of a healthy microbialite periphyton community sample imaged at 400x magnification. The greenish mass is a clump of *Euhalothece*. Also visible in association with the *Euhalothece* mat are a pennate diatom (arrow 1), filamentous organism (arrow 2), and green alga (arrow 3). Sample was collected October 10, 2019 from Site B. (D) Positive phase and differential interference contrast photomicrograph imaged at 1000x magnification of *Euhalothece* culture from a Great Salt Lake microbialite sample collected in 2019 at Antelope Island State Park **[6]**.

Great Salt Lake is currently threatened by a rapid decline in lake levels and consequent increase in salinity. Layered onto normal decadal cycles in precipitation [7], its watershed has been impacted by the megadrought that has gripped the western United States since 2000, which has been worsened by anthropogenic climate change [8]. An even greater threat to the lake, however, has been the overuse and diversion of the waters that would otherwise feed Great Salt Lake for agricultural, industrial, and municipal uses. Such consumptive water diversions are estimated to have reduced the lake's volume by >60% [9]. As a result, the lake has shrunk to historic low levels in the past decade (Fig 1E–F), following a pattern of water overuse leading to lake demise seen in ecologically-important saline lakes around the world [2,10]. Water overuse

in Great Salt Lake's watershed has substantially impaired the lake's resilience to future changes in regional hydroclimate [11]. It has become clear that, without an overhaul of water use policy and practice in the watershed, the lake could soon be lost [12].

Great Salt Lake's ecosystem-critical microbialites in peril

Meanwhile, low lake levels and consequent shoreline shift has exposed hundreds of kilometers of microbialite mounds, sometimes occurring in extensive reefs [5], a unique feature of Great Salt Lake's benthos. Microbialites, carbonate mounds formed by interactions of microbes with the lake's chemical environment, are of academic interest as analogues for economically important hydrocarbon reservoirs [13] and paleoenvironmental records [14–16]. Recently, it has also become apparent that they serve a critical function in the Great Salt Lake ecosystem. The microbial mat communities facilitate the production of calcium carbonate, and the structure that forms provides a solid, anchored, raised substrate on which productive microbial mats can grow—oases of stability among the shifting oolitic sands and carbonate mud that compose most of the Great Salt Lake benthos. Microbialite surface microbial communities (periphyton) conservatively represent one third of primary production in Great Salt Lake [17,18]. Microbialites provide the base of the lake's brine fly (*Ephydra* spp.) food chain; fly larvae depend on the microbialites for both food and pupation habitat [2,17,19–23]. The organisms that microbialite periphyton feed in turn feed millions of birds that depend on the lake ecosystem (Fig 2). Lake level fall is subjecting microbialites and their periphyton to desiccation.

In autumn 2022, roughly 40% of the lake's microbialites were subaerially exposed (Fig 1D, [5]) and desiccated (Figs 1G and 3), representing a substantial loss of productivity. A critical question for the management of Great Salt Lake and its associated watershed is how effectively

and under what conditions the microbialite periphyton communities persist. If policies are enacted that allow lake levels to rebound, do microbialite periphyton communities recover their ecosystem function? We investigated these questions during two successive summers where historic lake lowstands were reached and exceeded (2021 and 2022); this paper presents the findings along with other recent data on Great Salt Lake's microbialite periphyton communities.

Fig 3. Time series photographs from Buffalo Point field sites showing the effects of lake level fall. (A) Site B instrument pipe in July 2019 (left; top of pipe highlighted with arrow) vs. August 2021 (right). (B) Site B3 microbialite site in July 2021 (left) vs. July 2022 (right).

Materials and Methods

Field sites, time series data logging, and sample collection

The work described in this study focused on a microbialite reef on the northern end of Antelope Island in Great Salt Lake (Fig 1). GPS coordinates of all measurement and sample locations are provided in S5 Table. Time series water pressure, temperature, and downwelling irradiance were measured every 15 minutes collected using data loggers (temperature/pressure: HOBO® U20L, light/temperature: HOBO® MX2202, Onset® Computer Corporation) attached to a PVC pipe anchored to the lake bed. In March 2019, the instrument site was placed in 0.9 m deep water in a microbialite reef ~75 m from that date's shoreline (Site B; Fig 1G). In August 2021, Site B became subaerially exposed (Fig 3A) and the logger pipe was moved to a deeper site ~150 m farther lakeward from the 2019 shore (Site B3; Fig 1G). In addition, manual water

depth, visibility, salinity (using a handheld 0–28% refractometer with automatic temperature compensation; measurements are reported as a % by mass), density (using a brewing hydrometer), and temperature (using a digital aquarium thermometer) measurements were collected monthly to seasonally, along with microbialite surface observations. Lake elevation data were obtained from two U.S. Geological Survey monitoring sites in the lake's South Arm (Fig 1A), one near Saltair (ES1: Station 10010000), and the other on the railroad causeway (ES2: Station 10010024)[24]. Multiple manual field measurements of site water depths at each site were then used to determine depth offsets vs. lake level (i.e., site elevation).

Weather data

Weather data for 2019–November 2020 was obtained from a station on Antelope Island, located 4 km from the field site and operated by Antelope Island State Park (WS1: KUTSYRAC22, Ambient Weather WS-2090; Fig 1A); the station was non-operational beginning in November, 2020. Data for nearby stations available on WeatherUnderground (wunderground.com) were analyzed to find a new station with values consistent with those measured at KUTSYRAC22; S11 File); the station with the best coverage and closest similarity to KUTSYRAC22 was determined to be a private station located 14 km from the field site (WS2: KUTSYRAC27, Ambient Weather WS-2902; Fig 1A), with publicly available data retrieved and used in this study with permission from the station owner. For analytical purposes, measured weather values were averaged when data from both sites were available.

Microbialite field monitoring & core sampling

In addition to general observations collected during the long-term monitoring work, detailed systematic monitoring of microbialites at the study sites was conducted from July 27–August 17, 2021 and July 12–August 2, 2022 as part of the Weber State University GETUP (Geoscience Education Targeting Underrepresented Populations) Summer Research Experience program. Microbialites monitored in summer 2022 were additionally visited and sampled sporadically until October 20, 2022. For this work, microbialites were flagged for repeat photography and sampling. Each microbialite was photographed during each visit, and the location of different colored bands on each microbialite were measured using a homemade surveying device (S1 Appendix Fig S1.1). In 2022, monitored microbialites (in addition to logger Site B3 and recovery experiment Site RC) were located within a roped-off rectangle (quad) to protect them from foot traffic.

In 2022, core samples from microbialite tops were collected using 50 mL syringes with the tip cut off, extracted onto core cradles with a scale, and photographed. Cores were sectioned in the field into 1–2 cm top, middle, and bottom (deep) sections using a sterile scalpel, then stored in sterile 15 mL centrifuge tubes on ice for transport to the lab. Back in the lab, core subsections were ground to a paste with a sterilized mortar & pestle to homogenize, then aliquoted for microscopy and chlorophyll extraction as described below.

Recovery experiments

Recovery experiments involved submerging pieces of a desiccated microbialite back into lakewater, incubating for varying lengths of time, and recovering them for measurements of

community regrowth. The desiccated microbialite (t_0 control) was collected in October 2016 from the beach at Ladyfinger Point (Fig 1A) at roughly 1278.6 m elevation, indicating that it had been subaerially exposed for at least two years at the date of collection, after which it sat undisturbed and dry on a laboratory windowsill until its use in this experiment. The t_0 control microbialite was broken into 1–7 g pieces, which were placed into individual nylon mesh bags (mesh size = 350 μm) that were attached to submerged PVC anchors (S1 Appendix Fig S1.2). In 2021 (September 27–November 12), experiments were run at two sites: Site RA (near the edge of a microbialite reef with significant water movement), and Site RB (in the middle of a reef surrounded by microbialites with healthy periphyton), with samples collected at timepoints from 10–40 days. The experiment was repeated in 2022 (September 27–November 12) at Site RC (adjacent to logger instrument Site B3 in the middle of a different, initially healthy microbialite reef), with samples collected at timepoints from 0–100 days.

In 2021, samples collected at each timepoint were subsampled in the field for pigment and DNA extractions. Pigment subsamples were collected with surrounding lakewater in sterile 1.5 mL centrifuge tubes wrapped in electrical tape to minimize light exposure. DNA subsamples were collected by first swabbing an area of each sample and mixing the swab in DNeasy® PowerSoil® kit (Qiagen, Cat. # 12888-50) bead tubes that had been prepared with kit lysis solution. Then, a ~ 5 mm solid piece of each sample was also broken off using sterile tweezers and added to the same bead tube. Both pigment and DNA subsamples were flash-frozen on dry ice and stored frozen for transport. Back in the lab, DNA samples were thawed, vortexed for 5 minutes, and stored frozen at -20 °C until extracted following kit protocols (see S1 Appendix for additional protocol details). Pigment samples were processed immediately following the protocols described below.

In 2022, instead of processing samples in the field, samples were stored in sterile centrifuge tubes placed on ice for transport, and processed in the lab. Whole samples were then ground and processed following the pigment extraction and microscopy in the same manner described for the core samples.

Laboratory desiccation experiments

A submerged microbialite was collected near Site B3 in July, 2022, then placed in an incubator at 30 °C with one full-spectrum LED lamp (24W 3500 K full-spectrum lamp, Juhefa, Cat. # B08S7VSX6) and one UVA/UVB CFL lamp (23W 6500 K UVA/UVB lamp, Lucky Herp, Cat. # B082DYBQLL); spectra are copied in S1 Appendix Fig S1.3. The microbialite was allowed to desiccate for several days to weeks, and rinsed with distilled water at intervals between 6–52 days to simulate rain events. Microbialite surface coloration was measured immediately before and after rinsing events and periodically thereafter. Photographs were taken alongside a color card under standardized light conditions in order to measure surface coloration using the method described below. In addition, the dry mass of the microbialite was measured to assess removal of surface carbonate (weathering) during rinsing events.

Color analysis

Microbialite surface coloration—specifically, the relative amount of green—was measured as an indicator of surface pigmentation for field microbialites and the microbialite in the laboratory desiccation experiment, with lack of green indicating surface bleaching. To quantify coloration, photographs were taken of microbialite surfaces alongside a standard color

card (Pixel Perfect 24-Color Standard Calibration Chart). Color thresholding in ImageJ was then used to quantify the green pixels in an image, with a full protocol described in S1 Appendix.

Microscopy

Samples collected for microscopy were weighed (~0.2 g dry mass), vortexed with 1 mL of 2% PBS-buffered formaldehyde to fix, and stored at 4 °C. For both phase contrast and confocal laser scanning microscopy (CLSM), wet mount slides were prepared from ~60–100 µL of sample that had been vortexed to suspend solid material, using clear nail polish to seal coverslips to prevent water evaporation and salt precipitation. Brightfield and phase contrast microscopy photomicrographs were collected using an Accu-Scope® EXC-500 with an Excelsis MPX-16C camera and CaptaVision™ software. For confocal laser scanning microscopy (CLSM), 4',6-diamidino-2-phenylindole (DAPI, 1 µL of 1 µg·mL^{-1} stock in sterile, nuclease-free water; Thermo Scientific™ Cat. # 62248) and calcein (1 µL of 100 µg·mL^{-1} stock in sterile, nuclease-free water; Invitrogen™ Cat. # C481) fluorescent probes were added to the fixed sample prior to fixing cover slips, and fixed slides were stored in a dark box prior to analysis to prevent photobleaching. CLSM photomicrographs were imaged using an Olympus FV3000 with the following channels: DAPI, ex = 405 nm, em = 430–480 nm; calcein, ex = 488 nm, em = 500–540 nm; and chlorophyll, ex = 514 nm, em = 550–600 nm (full settings used for imaging are in S1 Appendix). For both phase contrast microscopy and CLSM, ten random photomicrographs were collected at 200x magnification for relative color/fluorescence analysis, and interesting features were photographed at various magnification; protocols for color/fluorescence analysis are described in detail in S1 Appendix. The *Euhalothece* culture in Fig 2D was imaged using an Olympus BX51 microscope using a DP27 5 MP capture card mounted on a U-TV1XC adaptor;

positive phase contrast and DIC were achieved by pairing an Olympus CX-PCD Phase Contrast condenser on Ph3 setting and Nomarsky DIC filter with a 100x objective.

Chlorophyll extractions

Chlorophyll extraction protocols used in 2021 and 2022 differed slightly in response to changes in equipment availability. In 2021, pigment samples were extracted by grinding solid samples to a powder using a sterile mortar and pestle, weighing the powder, then extracting overnight in 5 mL chilled, 100% acetone at 4 °C in 9 mL glass test tubes. The next day, the glass tubes were centrifuged inside 15 mL polypropylene centrifuge tubes for 5 minutes at 3000 g to sediment solids. The supernatant, containing polar pigments, was scanned in a 3.5 mL quartz cuvette (Vernier) from 500–800 nm at 1 nm spectral resolution and 0.1 $s \cdot \lambda^{-1}$ averaging using a UV-VIS spectrophotometer (Cary 60, Agilent).

In 2022, solid samples were weighed, added to 4 °C chilled 90% acetone in 1.5 mL opaque black polypropylene tubes (Argos Technologies™), vortexed 5 seconds to mix, and polar pigments were extracted overnight at 4 °C. Prior to measurement, samples were again vortexed, then centrifuged at 1000 g to sediment solids. Supernatant containing polar pigments was then scanned in a 400 µL quartz cuvette from 350–1000 nm at 1 nm spectral resolution and 0.1 s averaging using the UV-VIS spectrophotometer. Samples with dense concentrations of pigments (with peak absorbance readings > 2.0) were diluted with chilled 90% acetone prior to reading.

Chlorophyll *a* concentrations were then quantified using the equation described in Ritchie (2008), correcting for dilutions and normalizing to extracted sample mass.

DNA extraction, sequencing, and analysis

DNA extractions were performed using a DNeasy® PowerSoil® kit (Qiagen, Cat. # 12888-50), and extracted DNA was quantified fluorometrically (Qubit® 2.0 Fluorometer, Life Technologies) with a high-sensitivity, double-stranded DNA analysis kit (ThermoFisher Scientific Cat # Q32851). Sample barcoding, amplification, and pooling for both 16S and 18S SSU rRNA genes was performed per Earth Microbiome Project protocols (16S: Walters et al., 2016; 18S: Amaral-Zettler et al., 2009; Stoeck et al., 2010) by Wright Labs (Huntington, PA, USA). Amplicon sequencing was done, also by Wright Labs, using Illumina MiSeq v2 chemistry with paired-end 250 base pair reads for 16S, or 150 base pair reads for 18S. Sequences were deposited to the National Institute of Health's Sequence Read Archive (SRA) under BioSample accession SAMN32545145–SAMN32545168. Sequence analysis was performed using the Qiime2 pipeline [25], with details described in S1 Appendix.

Results

Depth, temperature, and salinity trends at the study site

Water depth, temperature, and salinity trends are summarized in Fig 4. Raw time series data are available in S6 File.

Fig 4. Environmental trends at microbialite reef field sites, 2019–2022. (A) Great Salt Lake elevation measurements (m-asl) at two USGS sites in the South Arm (left axis, lines), with manual depth measurements (right axis, circles) at Sites B and B3. (B) Air temperature (dashed lines) measured at KUTSYRAC22 (WS1) and KUTSYRAC27 (WS2), water temperature (solid lines) logged at the field site by three different data loggers, and manually measured temperatures (circles) at different water depths (water surface =top; middle depth = mid; sediment/water interface = bottom). (C) Downwelling (top) and sidewelling (side) irradiance logged at the field sites. (D) Daily accumulated precipitation measured at station KUTSYRAC22 (WS1) and KUTSYRAC27 (WS2). (E) Water salinity measured at different water depths (water surface = top; middle depth = mid; sediment/water interface = bottom); the October 2022 point was converted from density. In all plots, the shaded gray area indicates the move from Site B (left) to Site B3 (right, gray).

Changes in manual field site water depth measurements correlated closely with lake elevation changes when field sites remained hydrologically connected to the greater lake (Fig 4A). We were therefore able to estimate site elevations of 1277.26 m at Site B, 1277.0 at Sites RA and RB, and 1276.55 at Site B3 and RC. Using logged lake elevation data, we could then estimate site water depth over time during periods when sites were hydrologically open. Manual measurements were used when sites became hydrologically closed, which resulted in faster evaporation compared to the lake as a whole. Water depth at Site B declined by 0.95 m from July 2019 to July 2021, and declined an additional 0.10 m during the three weeks of microbialite desiccation monitoring in 2021, at which point the site became dry and the instrument pipe was moved to Site B3. Although some depth variability was recorded, there was no significant decline in water depth during the 2021 recovery experiment (Sites RA and RB), with a median

water depth of ~ 20 cm at both sites. Water depth declined 0.11 m at Sites B3 and RC during the three weeks of microbialite desiccation monitoring in 2022, and an additional 0.27 m during the remaining duration of the 2022 recovery experiments. The roped-off quad area containing instrument pipe B3, recovery experiment RC, monitored microbialites M1–M3, and cored microbialites C1–C3 became hydrologically closed toward mid-August, 2022, cut off from the greater lake by exposed microbialites.

Water temperature was strongly seasonal and mimicked trends in air temperatures (Fig 4B), ranging from -3.0 °C (measured January 3, 2022, when air temperature dropped as low as -7.9 °C) to +37.8 °C (measured July 31, 2022). Water temperatures were somewhat warmer during the 2022 microbialite monitoring season compared to the 2021 season (median temperature of 27.4 °C and 31.2 °C, respectively). Downwelling and sidewelling irradiance were also strongly seasonal (Fig 4C), and increased from 2021–2022, likely due to decreased water depth.

Total precipitation during the 2021 summer monitoring season was greater than during the 2022 monitoring season: 1.8 vs. 0.7 cm, respectively, with most of the rain during the 2021 monitoring season falling between the first and second monitoring weeks (Fig 4D). Total precipitation was also greater during the 2021 vs. 2022 recovery experiments: 9.6 vs. 5.0 cm, respectively, despite the substantially longer duration of the 2022 experiment.

Open-water salinity in the lakeward portion of the microbialite reef increased from 11.7% in July 2019 to 18.2% in July 2022, then to 19.5% in October 2022 (Fig 4E). Salinity proximal to the monitored microbialites was 16–17% during the 2021 monitoring season, 13–17% during the 2021 recovery experiments, 18–21% during the 2022 monitoring season, and 18–27% during the

2022 recovery experiments. Salinity in extensive, hydrodynamically restricted portions of the microbialite reef (including Sites B3 and RC) reached halite saturation in July 2022 (Fig 5), which became more widespread with lake elevation fall. Salinity measured using different techniques were closely correlated (S2 Appendix Fig S2.1); we therefore use refractometer measurements (% by weight) for the remainder of this paper except values ≥ 25 %, which were converted from lab density measurements using the equation of state from Naftz et al. [26]. For more discussion on the salinity and density measurements, see S2 Appendix.

Fig 5. Field photographs showing halite saturation in closed microbialite reef areas in 2022. (A) Halite lenses (arrows) forming on a closed portion of microbialite reef within 20 m of Site B3 in July, 2022. (B) Halite crystals coating a mesh bag from the recovery experiments at Site RC in September, 2022. (C) Photograph taken August 17, 2021 showing mm-scale halite crystals (white) covering the tops of microbialites following a windy (wave action) period. Abundant brine flies and fly pupal casings (dark) are also visible in the image.

Microbialite field monitoring and core sampling

Prolonged subaerial exposure results in surficial bleaching, a process by which microbialite surfaces change color from dark green to white, and display signs of weathering (Figs 3, 6, and 7). We observed initial stages of bleaching during both the 2021 and 2022 three-week intensive monitoring seasons (Figs 6, 7, and S12 Fig). Bleaching was quantifiable using image color analysis (Fig 6B). Quantitative results of surface monitoring are available in S7 File.

Over short timescales, bleaching was observed to be superficial, temporary, and influenced by water-soluble salts (especially halite); monitored microbialites re-greened following rain events (Figs 6 and S12 Fig), and samples collected were usually green just beneath the surface (< 1 cm). Indeed, microscopy revealed no obvious changes in surface samples, with *Euhalothece* clumps persisting in surface samples even in microbialites that appeared superficially bleached (Fig 8A).

Fig 6. Visible changes of microbialite surface over fourteen weeks of subaerial exposure. (A) Photographs of a single microbialite at Site B3 showing exposure, bleaching, and weathering during summer–autumn, 2022. Exposure times of each image match those in the graph below. (B) Surface coloration measurements of three monitored microbialites (green lines, left axis); points represent averages of three AOI measurements each week, with standard deviations represented as error bars. Also shown are daily accumulated precipitation amounts (blue bars, right axis). Note the bright discoloration (salt precipitation) in week 2, followed by re-greening in week 3 after a light rain event, then bleaching and weathering through week 14 after heavier rain.

Fig 7. Microbialite layer measurements. Summary of surface observations of microbialite bleaching and weathering, showing measurements of changing heights of microbialite color bands over a four-week period, overlaid by water depth at Site B3 (white line). Colors represent the approximate color of the observed bands. Values plotted are averages of multiple measurements from four microbialites. Error bars represent the standard deviation of twelve measurements for a single band.

Fig 8. Representative brightfield photomicrographs from core samples. Samples were collected from microbialite cores at Site B3 on July 12 (left images), August 2 (center images), and September 22 (right images), 2022. (A) Microbialite core top section samples. (B) Microbialite core bottom section samples. (C) Recovery experiment samples. In all images, the scale bar represents 100 μm. All images were manually adjusted for consistent white balance.

Beneath the surface, microbialite communities persisted following subaerial exposure, even showing increases in extractable chlorophyll and the amount of green cellular material visible in brightfield microscopy (Figs 8B and 9A–B). Consistent with this, chlorophyll channel CLSM fluorescence did not change significantly except for a general increase over time in bottom layer samples (Fig 9D). In contrast, DAPI channel fluorescence decreased over time in all layers (Fig 9C), and calcein channel fluorescence decreased in top and bottom layers (Fig 9E). All microbialite core measurements can be found in S9 File.

Fig 9. Microbialite core series results. Measurements from core top (T), middle (M), and bottom (B) sections; colors represent different timepoints: 0, 1, 2, 3, 10, and 14 weeks. (A) Extractable chlorophyll *a*. (B) Green material from brightfield microscopy random images as percent of total pixels. (C) DAPI, (D) chlorophyll, and (E) calcein channel fluorescence in CLSM random photomicrographs as percent of total pixels.

Lab desiccation experiments

Lab desiccation experiments accelerated, but otherwise mimicked field observations: surficial bleaching occurred rapidly, due at least in part to the accumulation of surface salts, and was immediately reversed upon rinsing with distilled water (Fig 10). Bleaching did, however, have an impact on microbialite weathering: during each rinse, surface material (which itself re-greened upon exposure to distilled water) sloughed off, and the microbialite lost dry mass. Material that was previously resistant to weathering was easily removed following each additional period of bleaching. Surface color measurements and masses are available in S8 File.

Fig 10. Lab desiccation experiment results. (A) Photograph series showing surficial changes to the microbialite, with days of exposure shown at bottom center of each image. (B) Surface green area analysis results (green line) with points representing the average measured fraction of green pixels in three AOIs for each date, and standard deviations shown as error bars, overlaid on measured microbialite mass (dashed line). Disturbance events are indicated along the top: rinse events are denoted with *, and a measurement following the removal of sandy surface material on day 49 is denoted with +. Note the loss of color over time, significant regreening following all rinse events, and weathering of surface material during disruption events.

Recovery experiments

Results in 2021

In 2021, we observed exponential increases in extractable chlorophyll and DNA over the 40-day period the experiment ran (Fig 11A–B; exponential best fit line r^2 values > 0.96 and 0.83, respectively), despite salinity levels exceeding 17% and falling water temperatures (Fig 4). In both cases, the growth rate was greater at the channel site (RA) vs. the reef interior site (RB). Extrapolating the exponential best fit lines to levels of chlorophyll *a* and DNA comparable to that of surrounding microbialites with healthy periphyton suggested a possible time to full recovery of ~60 and 90–130 days for RA and RB, respectively (Fig 11C–D).

Fig 11. Recovery experiment results. The top row shows extractable chlorophyll *a* (A), and DNA (B) with exponential best-fit lines (solid lines) shown along with r^2 values (in parentheses next to legend entries). Exponential recovery projections (dashed lines) based on chlorophyll and DNA are shown in (C) and (D), respectively. The bottom row shows extrapolations to "healthy" levels. The shaded region in C & D indicates the lower range of concentrations measured from healthy microbialite periphyton. RA and RB are from the experiments conducted in 2021, in a flowing channel vs. microbialite interior, respectively. RC is from the experiment conducted in 2022 in a reef interior site.

Results in 2022

The observed pattern in 2022 was different from what was observed in 2021. Although the extraction procedures used in 2022 differed somewhat from those used in 2021, precluding a direct comparison between values in the two experiments, no significant recovery trend was observed during the initial three weeks of the experiment (Fig 11A–B). However, a substantial increase in extractable chlorophyll was observed by incubation day 72, even though halite saturation had been reached (Fig 5B), and continued to increase through day 100 of the experiment (Fig 11A). Fitting an exponential best fit line indicated a slower rate of recovery than for the 2021 experiments (Fig 11C). Recovery experiment measurements are available in S9 File.

Community analysis from DNA sequencing

DNA sequencing results from the 2021 experiment indicated a consistent shift in community composition over time driven largely by a relative increase in Proteobacteria and Bacterioidota in bacterial 16S sequences (Fig 12A), and an increase in diatoms in eukaryotic 18S sequences (Fig 12B).

Fig 12. Recovery experiment DNA sequencing results. Results of 16S and 18S amplicon sequencing for the 2021 experiment at sites RA and RB, showing changes in microbial community over incubation time (numbers indicate incubation days) compared to lakewater and healthy microbialite periphyton (HM) samples. (A) Relative abundance of 16S sequencing ASVs belonging to different taxonomic groupings within the Bacteria and Archaea. *Most ASVs classed as *Dactylococcopsis* had closest sequence similarity to *Euhalothece*. (B) Relative abundance of 18S sequencing ASVs belonging to different taxonomic groupings within the Eukarya. (C) 16S and (D) 18S principal coordinate analysis (PcoA) plots of unweighted UniFrac sample distances showing the grouping of like samples (green = recovery experiment samples, blue = lakewater samples, red = healthy microbialite periphyton samples, gray = desiccated t_0 control samples) and the evolution of the recovery experiment communities over time (green arrow) away from the healthy periphyton community. The percentages of sample variance explained by each of the three displayed axes are shown next to the respective axis.

The community composition of control samples from a microbialite with a healthy periphyton was largely consistent with compositions found at other times and locations [6,16], and distinctly different from the composition found on the t_0 control microbialite used to seed the experiments (Fig 12). The difference between healthy periphyton and t_0 control was especially apparent in the 18S results, where the healthy periphyton control samples were dominated by *Artemia* sequences, which were absent from the bleached t_0 control microbialite and early recovery experiment samples, as well as from water compositions at different points during the experiment. Principal components ordinate analysis using unweighted UniFrac sample distances indicated that the shift in recovery community was *away* from the healthy periphyton

community, and more similar to water than healthy periphyton (Fig 12C). Amplicon sequence variant (ASV) tables of sequence abundance in each sample are reported in S10 File.

Analysis of cyanobacterial sequences

Cyanobacterial sequence abundance was low overall in our samples, likely the result of incomplete extraction, as cyanobacteria appeared to dominate sample biomass in microscopic examination (this is a commonly-reported issue for some cyanobacteria, especially in extreme environments [27,28]). DNA sequencing of the V4 region of the 16S rRNA gene produced a total of 14 ASVs representing 9 genera classified as belonging to the phylum Cyanobacteria, of which 10 were classified as belonging to the phylogenetic grouping of oxygenic photosynthetic cyanobacteria *sensu* Garcia-Pichel et al. [29], the others belonging to non-photosynthetic phyla. The greatest diversity in cyanobacterial sequences was found in lakewater samples. The desiccated t_0 control microbialite samples yielded no photosynthetic cyanobacterial ASVs; only one of the two replicates contained ASVs classified as belonging to the phylum Cyanobacteria, and those ASVs belonged to the Melainabacteria, a non-photosynthetic basal lineage [30,31].

A narrow phylogenetic cluster of three ASVs classified as *Dactylococcopsis* against the SILVA 138 database [32] dominated the healthy microbialite and recovery samples (S3 Appendix 9 Fig S3.1 and S10 File), making up >94% of cyanobacterial sequences in the dataset, and 100% of sequences in most recovery samples. This cluster will be referred to as *Euhalothece* for the remainder of this paper [33,34]. *Euhalothece* ASVs were relatively abundant in the control sample from a microbialite with a healthy periphyton, were present in some of the lakewater samples, absent in the desiccated t_o control sample, and appeared on recovery samples from both sites RA and RB by day 10.

The most abundant *Euhalothece* ASV (ASV1) had 100% sequence identity to several isolates of extremely halotolerant *Euhalothece* in the GenBank database [33,35], including the strain MPI 96N304 (AJ000713.1) mentioned in Lindsay et al. [36]. ASV1 was found in the healthy microbialite samples, all recovery experiment samples, and most lakewater samples. A second ASV (ASV2), which differed by only one base pair from ASV1 (S3 Appendix Table S3.2), represented 41–50% of the cyanobacterial sequences in the healthy microbialite periphyton control samples, but was only found in the healthy microbialite samples—not in lakewater or recovery experiment samples. A third ASV (ASV3) had 100% sequence identity over the region sequenced to Great Salt Lake *Cyanothece* sp. GSL007 (FJ546715.1), as well as several isolates of *Dactylococcopsis salina* isolated from salt pans in Salin de Giraud, France [37], and uncultured clones from Guerrero Negro, Mexico [38]. ASV3 made up between 6–25% of cyanobacterial sequences in five of seven Site RA recovery samples, and was only found in the Site RA recovery samples—not in healthy microbialite samples, lakewater, Site RB recovery experiment samples.

Discussion

Microbialite bleaching is initially superficial, with some endoliths persisting over months of subaerial exposure

Although decreases in surface coloration were observed over a several week period (Fig 6), with a white zone of bleaching extending gradually downward on the microbialites (Fig 7), pigment extracts and microscopy from core samples revealed that bleaching was initially

499 superficial, with substantial pigmented cellular material, including large *Euhalothece* clumps,
500 persisting even in the upper ~1 cm samples (Figs 8A and 9).

501 Both our lab experiments and field observations indicate that some apparent bleaching,
502 especially during early weeks of exposure, is attributable to the precipitation of reflective
503 evaporite minerals on microbialite surfaces during subaerial exposure and evaporation. This is
504 particularly obvious during periods of higher wave action, which can lead to the growth of mm-
505 scale halite crystals on microbialite surfaces (Fig 5C). These minerals can dissolve during rain
506 events, leading to a significant re-greening of microbialites that previously appeared bleached
507 (Figs 5, 9, and S12 Fig).

508 Initial increases in chlorophyll *a* and green-pigmented cells in deeper layers in the
509 microbialite indicate an endolithic survival strategy during subaerial exposure. Survival of
510 ordinarily surficial cyanobacteria and affiliated communities in deeper layers of permeable rock
511 during periods of subaerial exposure has been documented in other systems, including desiccated
512 lakes [39], and extracellular polymers (EPS) can aid in desiccation and freezing survival in
513 endolithic communities [40]. This is the first time to our knowledge that this growth habit has
514 been documented in the Great Salt Lake microbialites. However, the fraction of DAPI-
515 fluorescent cells decreased over time in all layers of the microbialite (up to the ~4 cm depth
516 measured), indicating that endolithic survival was not universal.

517 Microbialite bleaching enhances weathering

518 In longer-term observations of individual microbialites, substantial weathering was
519 observed following periods of bleaching (Figs 3, 6, 7, and S12 Fig). Upper portions of the
520 microbialites lose their robust, gooey/blubber-like quality over periods of prolonged exposure

and become loose and sandy, likely the direct consequence of declines in the surface microbial community and its affiliated EPS. Observable decreases in calcein fluorescence (Fig 9E), which binds to extracellular calcium and can therefore highlight degrading EPS, is consistent with this interpretation. The sandy carbonate material left on the desiccated surface is then easily weathered, as observed in the field and as illustrated in the observed mass loss following rinse events during the lab desiccation experiments (Fig 10). Enhanced weathering of the microbialites may be one of the longer-lasting consequences of microbialite exposure, as microbialite growth rates are not yet known in Great Salt Lake, but assumed to be quite slow [15].

Partial recovery of bleached microbialites occurs even at high salinity levels

The results of our recovery experiments in summer/autumn 2021 were broadly encouraging, showing an exponential rate of recovery when desiccated samples were re-submerged in lakewater at a salinity between 13–17%, as measured by extractable chlorophyll *a* and DNA (Figs 11A–B). If recovery continued along the same exponential trajectory, a full recovery to "healthy" values could occur within 120 days of being re-submerged, i.e., a single summer growth season (Figs 11C–D). Also encouraging was the appearance of *Euhalothece* sequences on the recovery samples after just 10 days incubation, as well as sequences of eukaryotic phototrophs (Figs 12A–B). Even if recovery did not proceed as quickly as our extrapolations predict, the combined results imply that a recovery of the ecosystem-critical microbialite primary producers is possible if microbialites—even badly bleached microbialites—are re-submerged in healthy lakewater.

When we repeated the experiment in the higher-salinity water of summer–autumn, 2022 (18–27%), recovery was markedly slower but did eventually appear to occur, with extracted chlorophyll *a* values reaching those seen in 2021 roughly seven weeks later, and increasing further in the following month (Fig 11A). *Euhalothece* clumps were visible in microscopic analyses in samples collected after 2–3 months incubation (Fig 8C), supplying additional evidence of recovery. This is remarkable, considering the salinity was at or near halite saturation when this apparent recovery was occurring. It is possible that the apparent recovery was simply a gradual accumulation of cells from the surrounding water (supported by the faster recovery rates of microbialites exposed to more lakewater flow; Fig 11A–B), which could potentially be preserved for some time by encrusting halite [41]. Additional work is required to determine whether the observed *Euhalothece* are actually photosynthetically active, or simply preserved.

Microbialites may be genetic islands

The unexpected diversity in sequences for the mat-forming unicellular cyanobacteria (*Euhalothece*) that dominate microbialite biomass and cyanobacterial sequences, as well as their spatial patterns found in this study, suggests that microbialites may serve as genetic islands, with different reef areas or perhaps even single microbialites hosting closely-related yet phylogenetically distinct organisms. Although the scope of this study was limited, it is notable that only one of the three *Euhalothece* ASVs appeared in lakewater sequences, even though they were abundant in recovery or healthy periphyton samples collected nearby. Whether this is a function of sampling, selection, or mutation cannot be determined from this study, but the result is intriguing nonetheless.

Microbialite recolonization likely depends on the health of the lakewater community

Recovery of the microbialite communities in our 2021 experiment (no DNA sequencing results are available for the 2022 experiments) appears to be based on recolonization from the surrounding water, rather than a 'resurrection' of dormant endolithic communities. Community distance analysis indicates that the microbial community present in recovery samples were more similar to lakewater than to either the desiccated microbialite t_0 community or the community present on microbialites with healthy periphyton (Figs 12C–D). The recovery sample communities that are most similar to lakewater were unsurprisingly those incubated for the shortest periods, and evolved away from lakewater over time, suggesting an initial seeding by lakewater. It is also notable that the 2021 recovery experiment site located in a channel away from the greater reef and exposed to more water flow (Site RA) experienced significantly faster recovery rates than was observed at the reef-interior site (RB).

The recovery sample community also evolved over time to become *less* similar to that seen in microbialites with healthy periphyton, despite the persistence of *Euhalothece*. Most notable is the relative dearth of Desulfobacterota in recovery experiment samples and high abundance of Flavobacteriales, Rhodobacterales, and Gammaproteobacteria, especially Marinobacteraceae and Oceanospirillales (Figs 12A–B). The low abundance of Desulfobacteria can be explained by the high salinity levels present during the recovery experiments; even halotolerant strains are not known to tolerate salinity levels above 13% [42,43]. It could, however, also be a consequence of an immature microbial mat lacking the anoxic zones required to support sulfur-reducing metabolisms. What is unclear is whether—given enough time and

development of a robust biofilm, then microbial mat—the community would begin to shift to more closely resemble that seen in microbialites with a healthy periphyton.

Primary seeding from lakewater indicates that microbialite recolonization is dependent on the health of the lakewater microbial ecosystem and the presence of viable *Euhalothece* and other organisms in lakewater. While microbialite communities may be able to survive, or at least be preserved, through periods of subaerial exposure and at high salinity, this is not true of lakewater communities. In the north arm, where salinity values routinely exceed 24%, *Euhalothece* sequences are absent [36], and the community composition is markedly different than that in the lake's south arm. Thus, a high-salinity lake would not be able to re-seed healthy microbialite periphyton communities. It appears that the lake's south arm is the ultimate reservoir for the organisms and metabolisms that support the broader Great Salt Lake ecosystem, including the microbialite microbial communities.

Conclusions

Great Salt Lake's microbialites and their surface microbial communities are in peril from declining lake water levels and a concurrent increase in the salinity of the lake, which is amplified in hydrologically closed areas of microbialite reef. In recent years, dramatic bleaching of newly-exposed microbialites has been observed, causing concern about the future of the microbialites and impacts on the broader ecosystem. Here, we have shown that microbialite bleaching is initially superficial, with an endolithic survival mode allowing the microbialite communities to be resilient for months after surface bleaching is observed. We also showed that portions of the microbialite surface communities, including the ecosystem-critical cyanobacterial component, can recover when bleached, desiccated microbialites are re-submerged and seeded

by healthy lakewater communities. In other words, if lake level rebounds, microbialite periphyton communities and their ecosystem function can potentially recover (Fig 13).

Fig 13. Summary of the big-picture findings of this study. The left panel shows a healthy Great Salt Lake ecosystem at an elevation of roughly 1279 m, where microbialites are mostly submerged and salinity levels are moderate. The center panel shows the state of the lake in summer–autumn 2022, where vast expanses of microbialite reef were subaerially exposed and salinity was high, resulting in a substantial decrease in the health and productivity of microbialite periphyton and reduced brine fly pupae anchor sites, as well as weathering of exposed microbialites. The right panel illustrates a potential future where lake levels continue to decline and salinity continues to increase, similar to what is seen in the modern north arm of the lake, where microbialites no longer support a healthy, productive periphyton and other key members of the ecosystem are absent due to exceeded salinity thresholds. Rapid lake rebound could result in the recovery of the microbialite-supported ecosystem so long as salinity levels do not preclude the survival of recolonizing organisms.

However, microbialite surface communities are not quite "just add water" communities: to re-seed, they require the right water, consisting of a healthy microbial community, which necessitates salinity levels that are lower than what is anticipated if lake level continues to fall or if freshwater input remains low. In addition, prolonged periods of subaerial exposure result in enhanced weathering of the microbialites, brushing off carbonate growth that may have taken centuries to form, and shrinking the overall height and surface area of these structures. This could have consequences for productivity in an otherwise healthy lake: less microbialite surface

area means less area that can host productive periphyton, and less area on which brine fly larvae can anchor.

Much remains to be elucidated in this system. Can re-submerged microbialites make a full recovery, and how long does it take? What are the conditions under which recovery can occur? Is the persistence of chlorophyll and DNA seen in deeper layers of the microbialite indicative of a healthy endolithic community, or simply preservation in halite? Which microbialite residents are truly critical to support the greater Great Salt Lake ecosystem? Are more ancient layers of the microbialite more resistant to weathering? And if so, what processes led to their more robust lithification that are different from what we have seen since the last time the microbialites were exposed *en masse*?

The big-picture message of this study is a hopeful, yet urgent one: if changes in human water use can result in more freshwater flowing back into the lake soon, we can still expect to see a recovery of microbialite-supported primary productivity. However, if lake level continues to decline, producing further increases in lake salinity prior to a rebound in lake level, desiccated microbialites may not re-seed with their chief primary producers. Indeed, microbialites in the salt-saturated north arm of Great Salt Lake no longer support a cyanobacterial periphyton [36]. Meanwhile, the longer already-exposed microbialites remain exposed, the more they will weather, potentially decreasing their future capacity to contribute to the Great Salt Lake ecosystem. Thus, the time to act is now.

Acknowledgements

Sampling at Great Salt Lake was done under Utah Department of Natural Resources permit #410-00736 and equivalent earlier permits, as well as a MOU with Antelope Island State

Park, which also provided access to KUTSYRAC22 weather data. KUTSYRAC27 weather station data was obtained with permission from the owners (Thompson family). We acknowledge the use of imagery from the NASA Worldview application (https://worldview.earthdata.nasa.gov), part of the NASA Earth Observing System Data and Information System (EOSDIS). Microbialite layer measurements reported in this study were done by Jared Gibby. Jake Aeschlimann assisted with DNA sequence analysis. We gratefully acknowledge instrumentation support at Weber State from Leigh Komperda, Elizabeth Sandquist, Michele Culumber, and Marek Matyjasik, logistical support from Ross LaRue, and administrative support from Ana Cich. CF would also like to acknowledge the numerous Weber State undergraduate student researchers, past and present, who inspired and informed early work that led to the projects presented here, especially Celina Patiño, Charise Penrod, and Aybree DeGrange.

References

1. WHSRN. Great Salt Lake - Western Hemisphere Shorebird Reserve Network. In: Great Salt Lake [Internet]. 9 Jan 2023 [cited 3 Feb 2023]. Available: https://whsrn.org/whsrn_sites/great-salt-lake/
2. Conover MR, Bell ME. Importance of Great Salt Lake to Pelagic Birds: Eared Grebes, Phalaropes, Gulls, Ducks, and White Pelicans. In: Baxter BK, Butler JK, editors. Great Salt Lake Biology: A Terminal Lake in a Time of Change. Cham: Springer International Publishing; 2020. pp. 239–262. doi:10.1007/978-3-030-40352-2_8
3. Sorensen ED, Hoven HM, Neill J. Great Salt Lake Shorebirds, Their Habitats, and Food Base. In: Baxter BK, Butler JK, editors. Great Salt Lake Biology: A Terminal Lake in a Time of Change. Cham: Springer International Publishing; 2020. pp. 263–309. doi:10.1007/978-3-030-40352-2_9
4. Marden B, Brown P, Bosteels T. Great Salt Lake Artemia: Ecosystem Functions and Services with a Global Reach. In: Baxter BK, Butler JK, editors. Great Salt Lake Biology: A Terminal Lake in a Time of Change. Cham: Springer International Publishing; 2020. pp. 175–237. doi:10.1007/978-3-030-40352-2_7
5. Baskin RL, Della Porta G, Wright VP. Characteristics and controls on the distribution of sublittoral microbial bioherms in Great Salt Lake, Utah: Implications for understanding microbialite development. Depositional Rec. 2022;8: 39–66. doi:10.1002/dep2.159

6. Kanik M, Munro-Ehrlich M, Fernandes-Martins MC, Payne D, Gianoulias K, Keller L, et al. Unexpected Abundance and Diversity of Phototrophs in Mats from Morphologically Variable Microbialites in Great Salt Lake, Utah. Atomi H, editor. Appl Environ Microbiol. 2020;86: e00165-20. doi:10.1128/AEM.00165-20
7. Wang S-Y, Gillies RR, Jin J, Hipps LE. Coherence between the Great Salt Lake Level and the Pacific Quasi-Decadal Oscillation. J Clim. 2010;23: 2161–2177. doi:10.1175/2009JCLI2979.1
8. Williams AP, Cook ER, Smerdon JE, Cook BI, Abatzoglou JT, Bolles K, et al. Large contribution from anthropogenic warming to an emerging North American megadrought. Science. 2020;368: 314–318. doi:10.1126/science.aaz9600
9. Null SE, Wurtsbaugh WA. Water Development, Consumptive Water Uses, and Great Salt Lake. In: Baxter BK, Butler JK, editors. Great Salt Lake Biology: A Terminal Lake in a Time of Change. Cham: Springer International Publishing; 2020. pp. 1–21. doi:10.1007/978-3-030-40352-2_1
10. Wurtsbaugh WA, Miller C, Null SE, DeRose RJ, Wilcock P, Hahnenberger M, et al. Decline of the world's saline lakes. Nat Geosci. 2017;10: 816–821. doi:10.1038/ngeo3052
11. Hassan D, Burian SJ, Johnson RC, Shin S, Barber ME. The Great Salt Lake Water Level is Becoming Less Resilient to Climate Change. Water Resour Manag. 2022 [cited 31 Jan 2023]. doi:10.1007/s11269-022-03376-x
12. Abbott BW, Baxter BK, Busche K, de Freitas L, Frei R, Gomez T, et al. Emergency measures needed to rescue Great Salt Lake from ongoing collapse. Provo, Utah: Brigham Young University; 2023 Jan p. 34. Available: https://pws.byu.edu/great-salt-lake
13. Chidsey TC, Vanden Berg MD, Eby DE. Petrography and characterization of microbial carbonates and associated facies from modern Great Salt Lake and Uinta Basin's Eocene Green River Formation in Utah, USA. Geol Soc Lond Spec Publ. 2015;418: 261–286. doi:10.1144/SP418.6
14. Bouton A, Vennin E, Boulle J, Pace A, Bourillot R, Thomazo C, et al. Linking the distribution of microbial deposits from the Great Salt Lake (Utah, USA) to tectonic and climatic processes. Biogeosciences. 2016;13: 5511–5526. doi:10.5194/bg-13-5511-2016
15. Newell DL, Jensen JL, Frantz CM, Vanden Berg MD. Great Salt Lake (Utah) Microbialite $\delta^{13}C$, $\delta^{18}O$, and $\delta^{15}N$ Record Fluctuations in Lake Biogeochemistry Since the Late Pleistocene. Geochem Geophys Geosystems. 2017;18: 3631–3645. doi:10.1002/2017GC007078
16. Ingalls M, Frantz CM, Snell KE, Trower EJ. Carbonate facies-specific stable isotope data record climate, hydrology, and microbial communities in Great Salt Lake, UT. Geobiology. 2020;18: 566–593. doi:10.1111/gbi.12386
17. Wurtsbaugh WA, Gardberg J, Izdepski C. Biostrome communities and mercury and selenium bioaccumulation in the Great Salt Lake (Utah, USA). Sci Total Environ. 2011;409: 4425–4434. doi:10.1016/j.scitotenv.2011.07.027
18. Anderson NL, Barrett KL, Jones SE, Belovsky GE. Impact of abiotic factors on microbialite growth (Great Salt Lake, Utah, USA): a tank experiment. Hydrobiologia. 2020;847: 2113–2122. doi:10.1007/s10750-020-04235-9
19. Barrett KL. Microbialite communities and food web linkages in Great Salt Lake. Notre Dame. 2020.
20. Collins N. Population ecology of Ephydra cinerea Jones (Diptera: Ephydridae), the only benthic metazoan of the Great Salt Lake, U.S.A. Hydrobiologia. 1980;68: 99–112.

doi:10.1007/BF00019696

21. Caudell JN, Conover MR. Energy content and digestibility of brine shrimp (*Artemia franciscana*) and other prey items of eared grebes (*Podiceps nigricollis*) on the Great Salt Lake, Utah. Biol Conserv. 2006;130: 251–254. doi:10.1016/j.biocon.2005.12.018
22. Belovsky GE, Stephens D, Perschon C, Birdsey P, Paul D, Naftz D, et al. The Great Salt Lake Ecosystem (Utah, USA): long term data and a structural equation approach. Ecosphere. 2011;2: art33. doi:10.1890/ES10-00091.1
23. Brown PD, Craine JM, Richards D, Chapman A, Marden B. DNA metabarcoding of the phytoplankton of Great Salt Lake's Gilbert Bay: Spatiotemporal assemblage changes and comparisons to microscopy. J Gt Lakes Res. 2022;48: 110–124. doi:10.1016/j.jglr.2021.10.016
24. U.S. Geological Survey. USGS Water Data for the Nation. 2022 [cited 31 Jan 2023]. Available: https://waterdata.usgs.gov/nwis
25. Bolyen E, Rideout JR, Dillon MR, Bokulich NA, Abnet CC, Al-Ghalith GA, et al. Reproducible, interactive, scalable and extensible microbiome data science using QIIME 2. Nat Biotechnol. 2019;37: 852–857. doi:10.1038/s41587-019-0209-9
26. Naftz DL, Millero FJ, Jones BF, Green WR. An Equation of State for Hypersaline Water in Great Salt Lake, Utah, USA. Aquat Geochem. 2011;17: 809–820. doi:10.1007/s10498-011-9138-z
27. Garcia-Pichel F, López-Cortés A, Nübel U. Phylogenetic and Morphological Diversity of Cyanobacteria in Soil Desert Crusts from the Colorado Plateau. Appl Environ Microbiol. 2001;67: 1902–1910. doi:10.1128/AEM.67.4.1902-1910.2001
28. Bernardo, Alcántara-Hernández RJ, Montejano G, López-Martínez R, Falcón LI, Becerra-Absalón I. Cyanobacteria in microbialites of Alchichica Crater Lake: a polyphasic characterization. Eur J Phycol. 2021;56: 428–443. doi:10.1080/09670262.2020.1853815
29. Garcia-Pichel F, Zehr JP, Bhattacharya D, Pakrasi HB. What's in a name? The case of cyanobacteria. J Phycol. 2020;56: 1–5. doi:10.1111/jpy.12934
30. Di Rienzi SC, Sharon I, Wrighton KC, Koren O, Hug LA, Thomas BC, et al. The human gut and groundwater harbor non-photosynthetic bacteria belonging to a new candidate phylum sibling to Cyanobacteria. Kolter R, editor. eLife. 2013;2: e01102. doi:10.7554/eLife.01102
31. Soo RM, Hemp J, Parks DH, Fischer WW, Hugenholtz P. On the origins of oxygenic photosynthesis and aerobic respiration in Cyanobacteria. Science. 2017;355: 1436–1440. doi:10.1126/science.aal3794
32. Yilmaz P, Parfrey LW, Yarza P, Gerken J, Pruesse E, Quast C, et al. The SILVA and "All-species Living Tree Project (LTP)" taxonomic frameworks. Nucleic Acids Res. 2014;42: D643–D648. doi:10.1093/nar/gkt1209
33. Garcia-Pichel F, Nübel U, Muyzer G. The phylogeny of unicellular, extremely halotolerant cyanobacteria. Arch Microbiol. 1998;169: 469–482. doi:10.1007/s002030050599
34. Margheri MC, Ventura S, Kaštovský J, Komárek J. The taxonomic validation of the cyanobacterial genus Halothece. Phycologia. 2008;47: 477–486. doi:10.2216/07-87.1
35. Sayers EW, Bolton EE, Brister JR, Canese K, Chan J, Comeau DC, et al. Database resources of the national center for biotechnology information. Nucleic Acids Res. 2022;50: D20–D26. doi:10.1093/nar/gkab1112
36. Lindsay MR, Anderson C, Fox N, Scofield G, Allen J, Anderson E, et al. Microbialite response to an anthropogenic salinity gradient in Great Salt Lake, Utah. Geobiology.

2017;15: 131–145. doi:10.1111/gbi.12201

37. Hamlaoui S, Yéprémian C, Duval C, Marie B, Djédiat C, Piquet B, et al. The Culture Collection of Cyanobacteria and Microalgae at the French National Museum of Natural History: A Century Old But Still Alive and Kicking! Including in Memoriam: Professor Alain Couté. Cryptogam Algol. 2022;43: 41–83. doi:10.5252/cryptogamie-algologie2022v43a3
38. Kirk Harris J, Gregory Caporaso J, Walker JJ, Spear JR, Gold NJ, Robertson CE, et al. Phylogenetic stratigraphy in the Guerrero Negro hypersaline microbial mat. ISME J. 2013;7: 50–60. doi:10.1038/ismej.2012.79
39. Sánchez-Sánchez J, Cerca M, Alcántara-Hernández RJ, Lozano-Flores C, Carreón-Freyre D, Levresse G, et al. Extant microbial communities in the partially desiccated Rincon de Parangueo maar crater lake in Mexico. FEMS Microbiol Ecol. 2019;95: fiz051. doi:10.1093/femsec/fiz051
40. Knowles EJ, Castenholz RW. Effect of exogenous extracellular polysaccharides on the desiccation and freezing tolerance of rock-inhabiting phototrophic microorganisms: Effect of EPS on tolerance of rock-inhabiting phototrophs. FEMS Microbiol Ecol. 2008;66: 261–270. doi:10.1111/j.1574-6941.2008.00568.x
41. Perl SM, Baxter BK. Great Salt Lake as an Astrobiology Analogue for Ancient Martian Hypersaline Aqueous Systems. In: Baxter BK, Butler JK, editors. Great Salt Lake Biology: A Terminal Lake in a Time of Change. Cham: Springer International Publishing; 2020. pp. 487–514. doi:10.1007/978-3-030-40352-2_16
42. Brandt KK, Ingvorsen K. Desulfobacter halotolerans sp. nov., a Halotolerant Acetate-Oxidizing Sulfate-Reducing Bacterium Isolated from Sediments of Great Salt Lake, Utah. Syst Appl Microbiol. 1997;20: 366–373. doi:10.1016/S0723-2020(97)80004-5
43. Qian Z, Tianwei H, Mackey HR, van Loosdrecht MCM, Guanghao C. Recent advances in dissimilatory sulfate reduction: From metabolic study to application. Water Res. 2019;150: 162–181. doi:10.1016/j.watres.2018.11.018

Supporting information

S1 Appendix. Detailed methods. Includes additional details for microbialite surface layer measurements, the recovery experiment field setup, lab desiccation experiment lamps, CLSM settings, image analysis protocols, and DNA extraction, amplification, sequencing, and analysis protocols.

S2 Appendix. Discussion of salinity measurements. Comparison and discussion of refractometer, field density, and lab density measurements of lakewater salinity.

S3 Appendix. Cyanobacterial sequence analysis results. Bar plot of cyanobacterial ASV frequency in our samples, and a table of *Euhalothece* ASV sequences highlighting base pair differences.

S4 Appendix. List of supplemental results on Open Science Framework.

S5 Table. Field sites. Locations referred to in this paper, including sampling locations and logger sites. Excel (xlsx) file.

S6 File. Time series data. Time series field data for lake elevation, weather, and water temperature, light, and salinity. Includes logger data as well as manual field measurements. Excel (xlsx) file.

S7 File. Microbialite surface layer and % green measurements. Measurements of microbialite layers from monitored microbialites, and % green values calculated from photographs of microbialites M1–M3. Excel (xlsx) file.

S8 File. Lab desiccation experiment results. Measurements of surface %green and mass from the lab microbialite desiccation experiment. Excel (xlsx) file.

S9 File. Microscopy and extract results. Sample information and measurements of extractable DNA, pigment spectra and calculated chlorophyll *a* concentrations, and color analyses for brightfield and confocal microscopy. Includes measurements from microbialite cores and recovery experiment samples. Excel (xlsx) file.

S10 File. Recovery experiment ASV tables. Amplicon sequence variant tables for results of 16S and 18S rRNA gene sequencing. Includes raw counts, normalized abundance, and grouped abundance. Excel (xlsx) file.

S11 File. Weather station comparison. Weather station data from eight weather stations with publicly available data nearby to the Antelope Island field site. Web (html) file with interactive plots generated using bokeh for python (v. 2.3.3, bokeh.org).

S12 Fig. Time series field photographs of monitored microbialites. Time series photomicrographs showing the initial stages of bleaching of several different microbialites over time. Numbers represent the number of days the microbialites were subaerially exposed when the photo was taken. All microbialites shown were located near Site B3. (A) Microbialite M6, (B) Microbialite M5, and (C) Microbialite M13 monitored in July–August 2021. (D) Microbialite M1, (E) Microbialite M2, and (F) Microbialite M3 monitored in July–August 2022. Features of note include bright gray halite mineral formation visible in the latter panels of A & B and the 14-day panels of E–F, weathering in the 13 day panel of C, and re-greening following rain events in the 21-day panels of E–F.

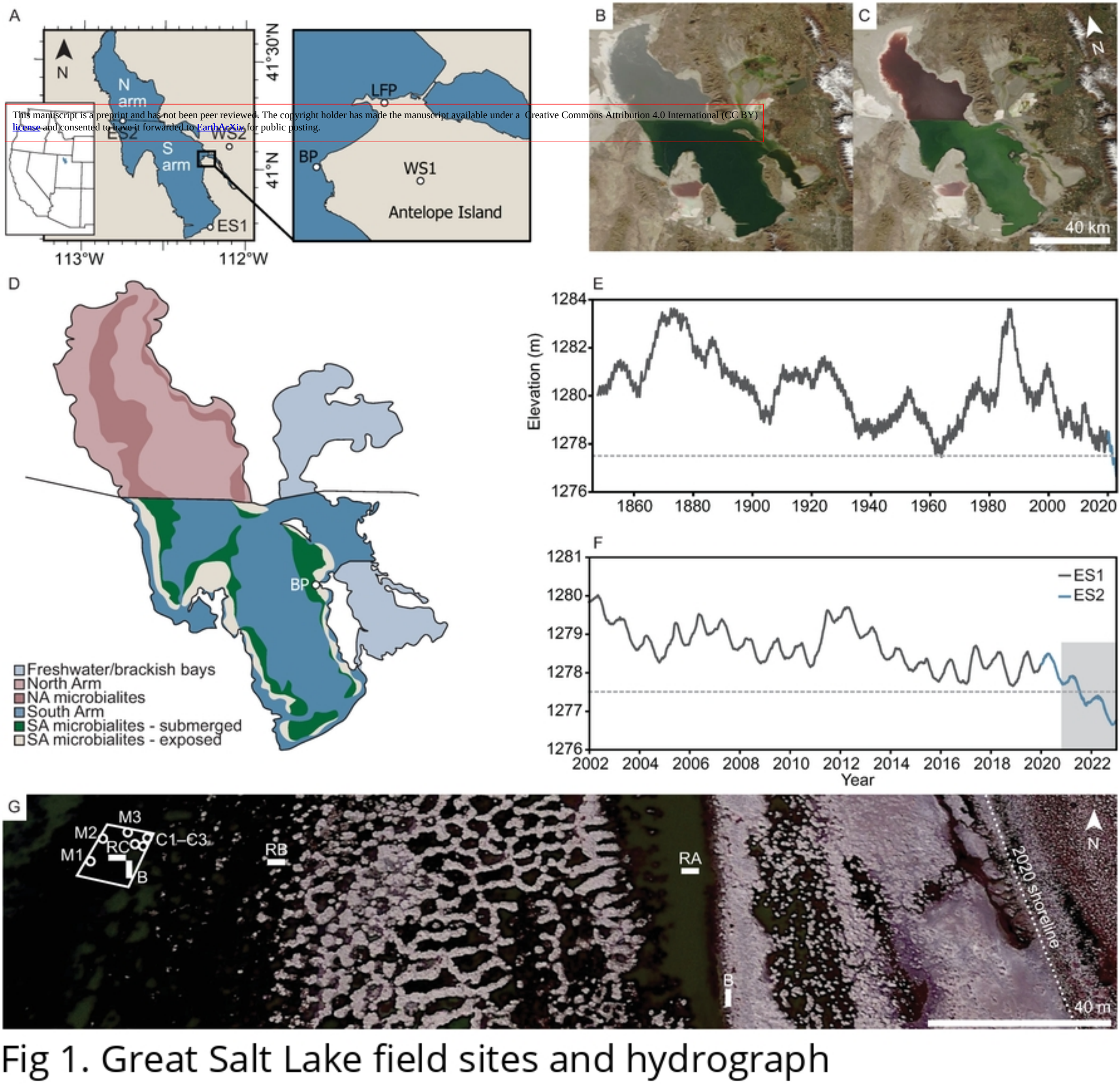

Fig 1. Great Salt Lake field sites and hydrograph

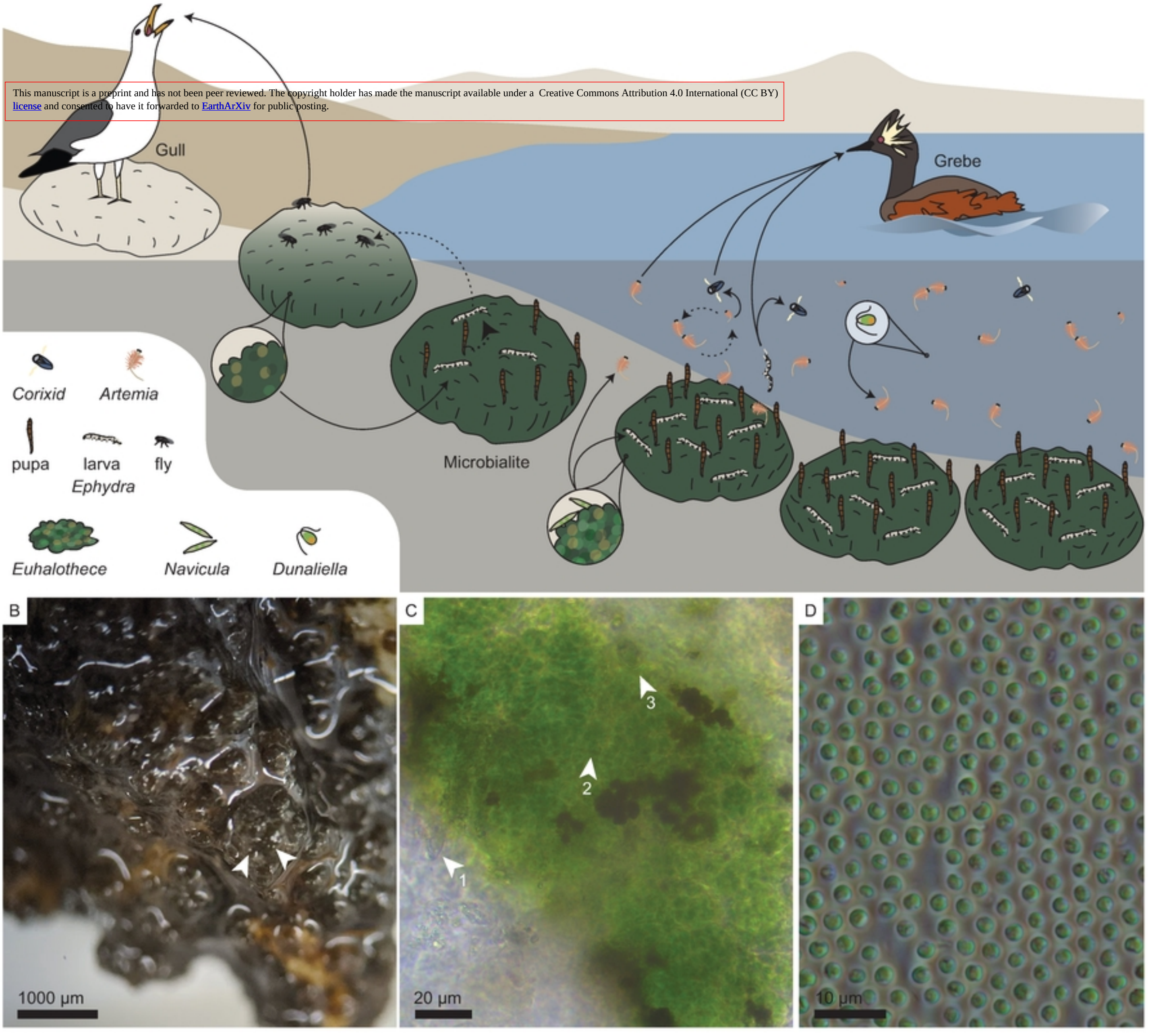

Fig 2. Great Salt Lake's microbialite-supported ecosystem

Fig 3. Time series photographs from Buffalo Point field sites sho

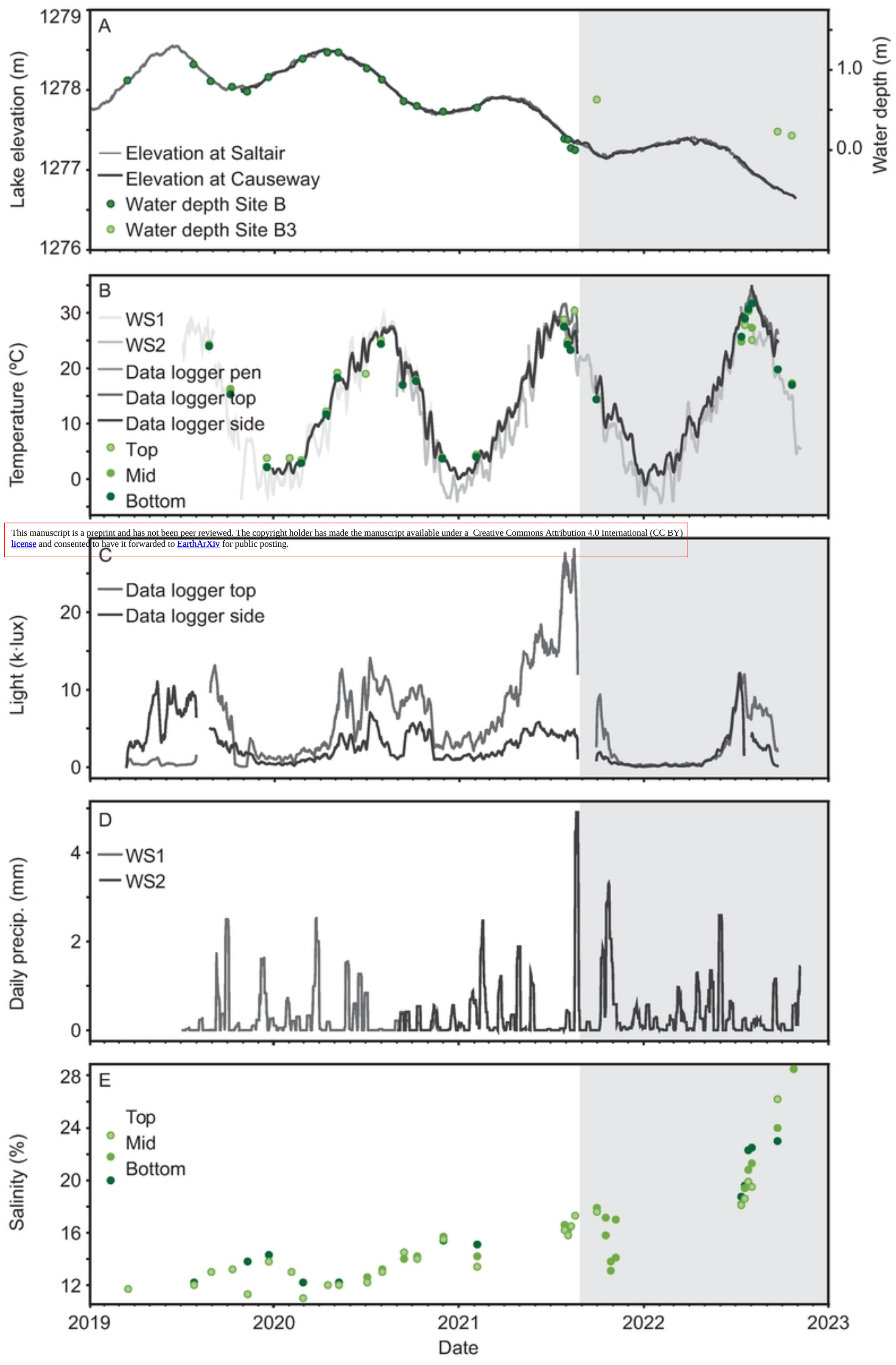

Fig 4. Environmental trends at microbialite reef field sites

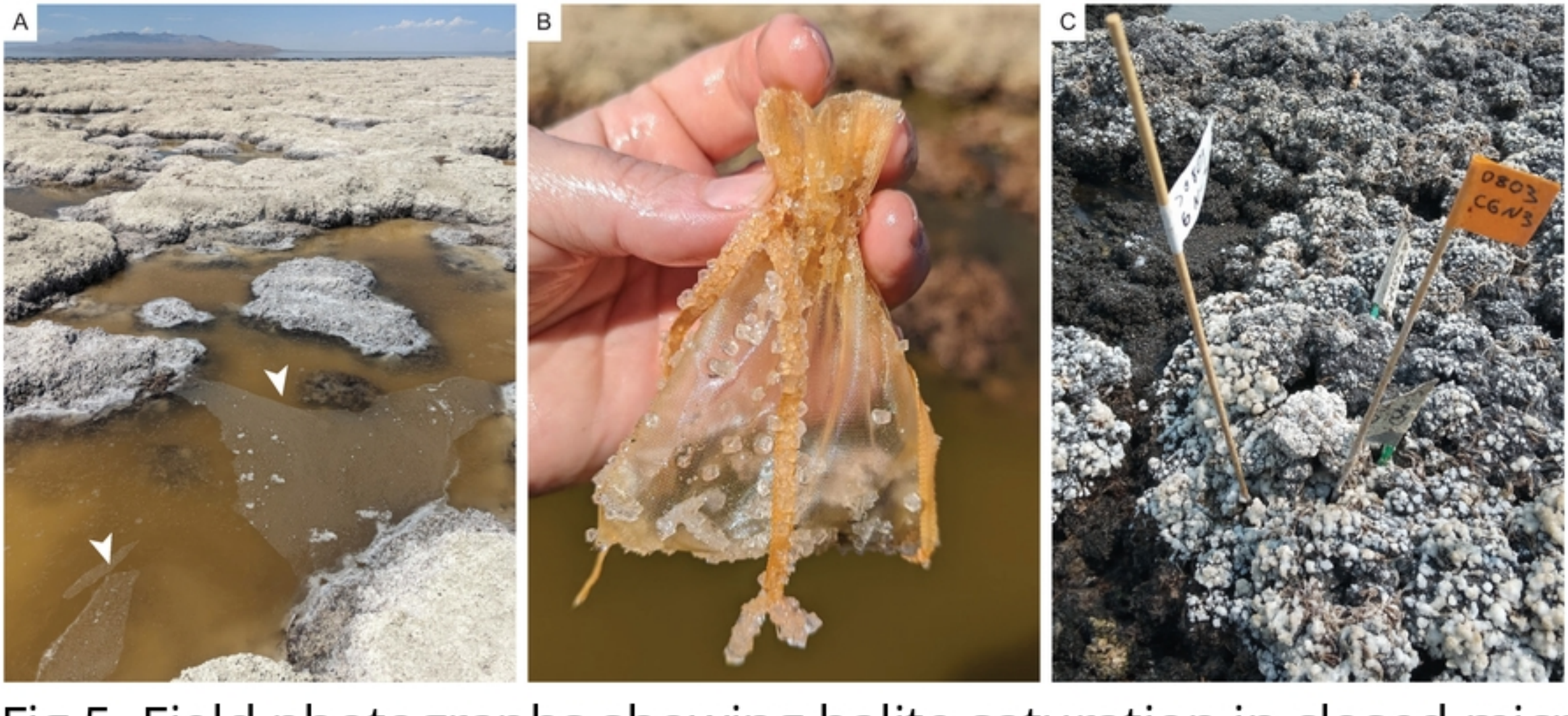

Fig 5. Field photographs showing halite saturation in closed micr

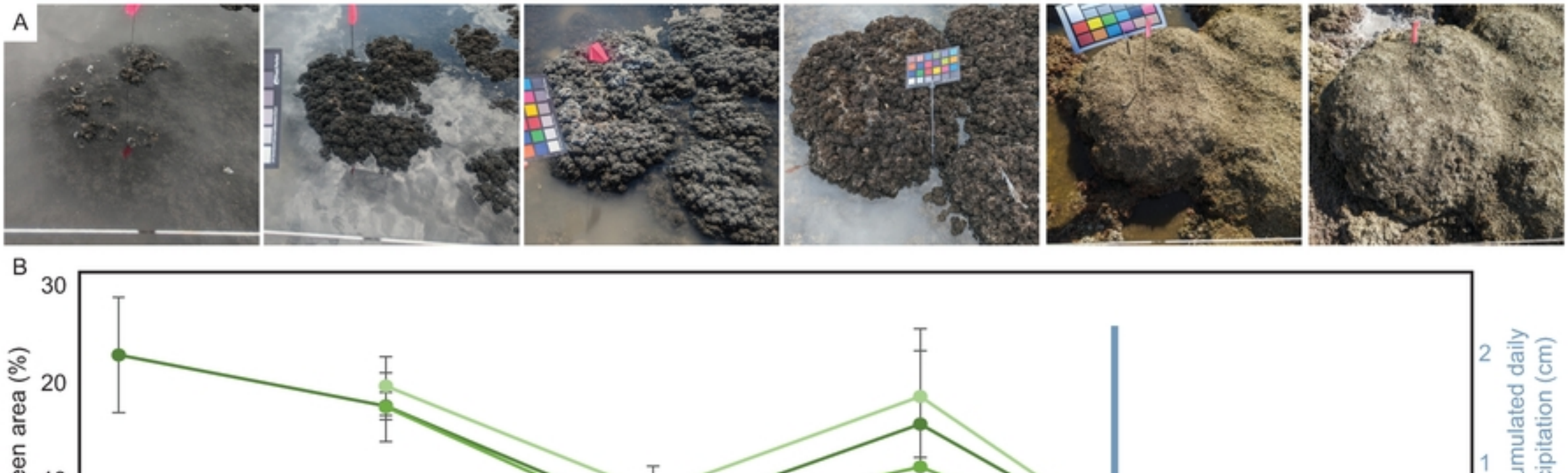

Fig 6. Visible changes of microbialite surface over fourteen week

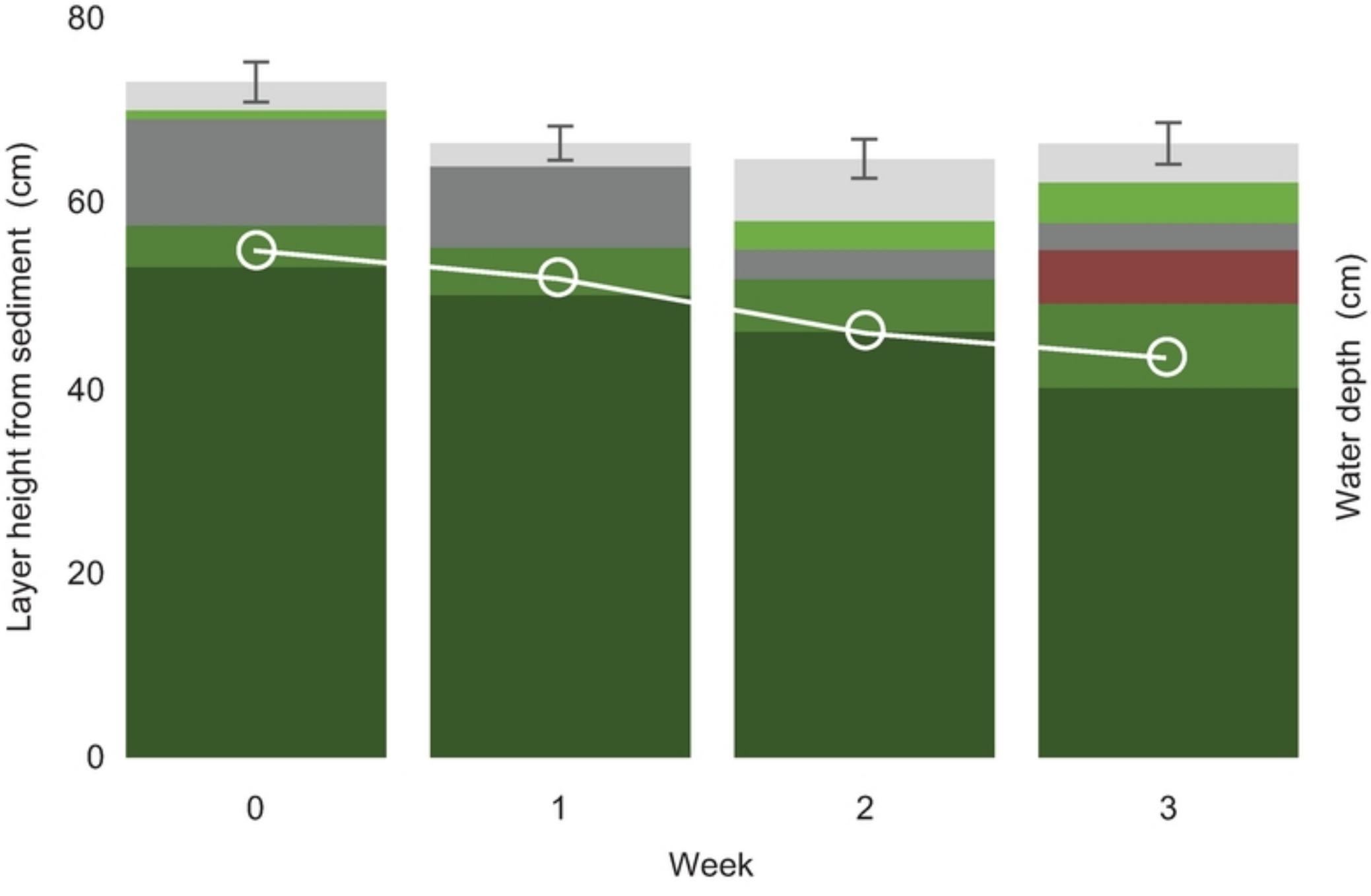

Fig 7. Microbialite layer measurements

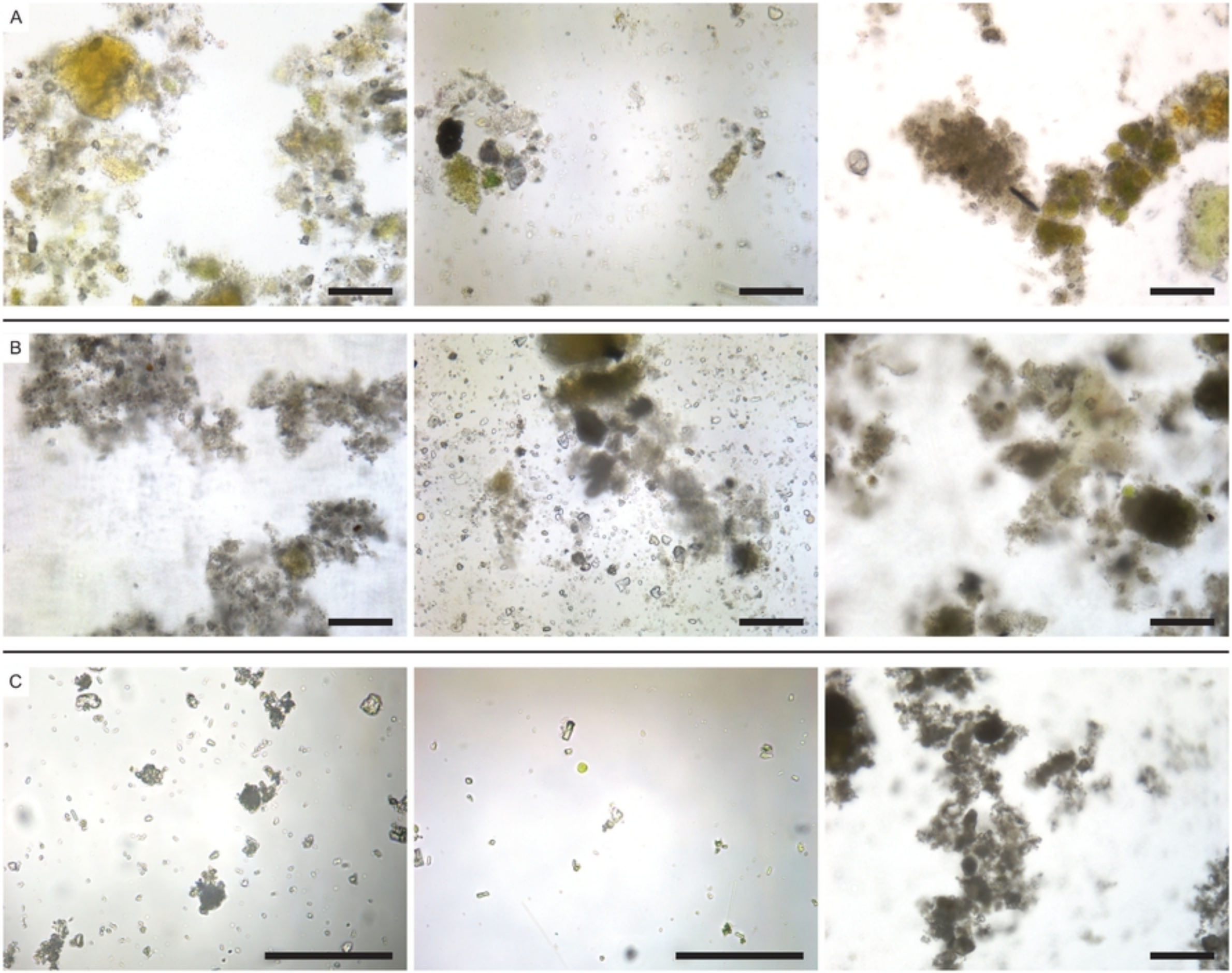

Fig 8. Representative brightfield photomicrographs from core sa

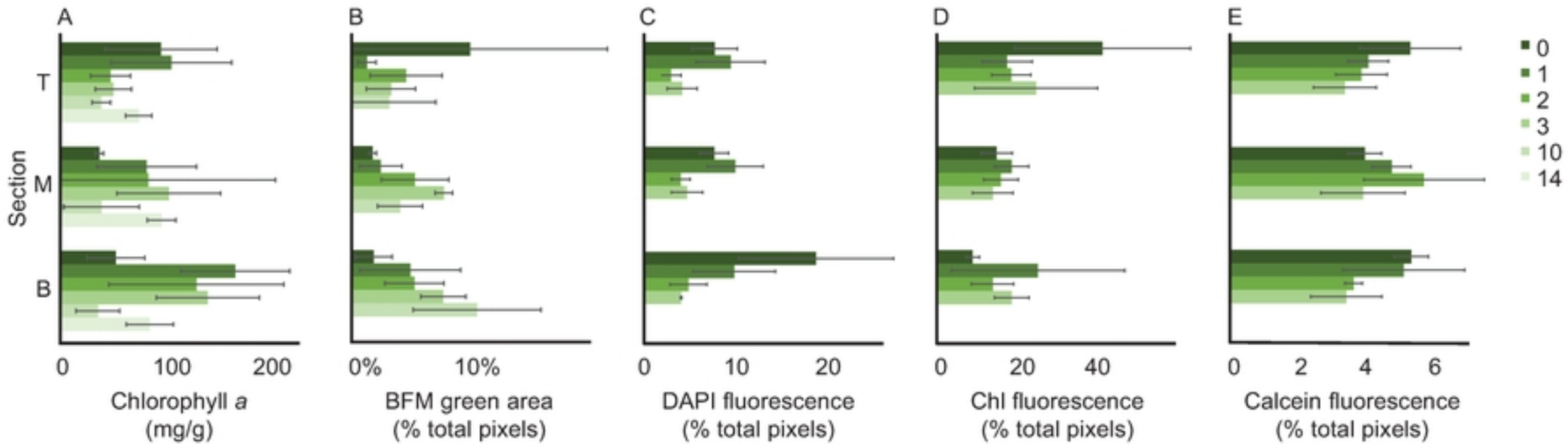

Fig 9. Microbialite core series results

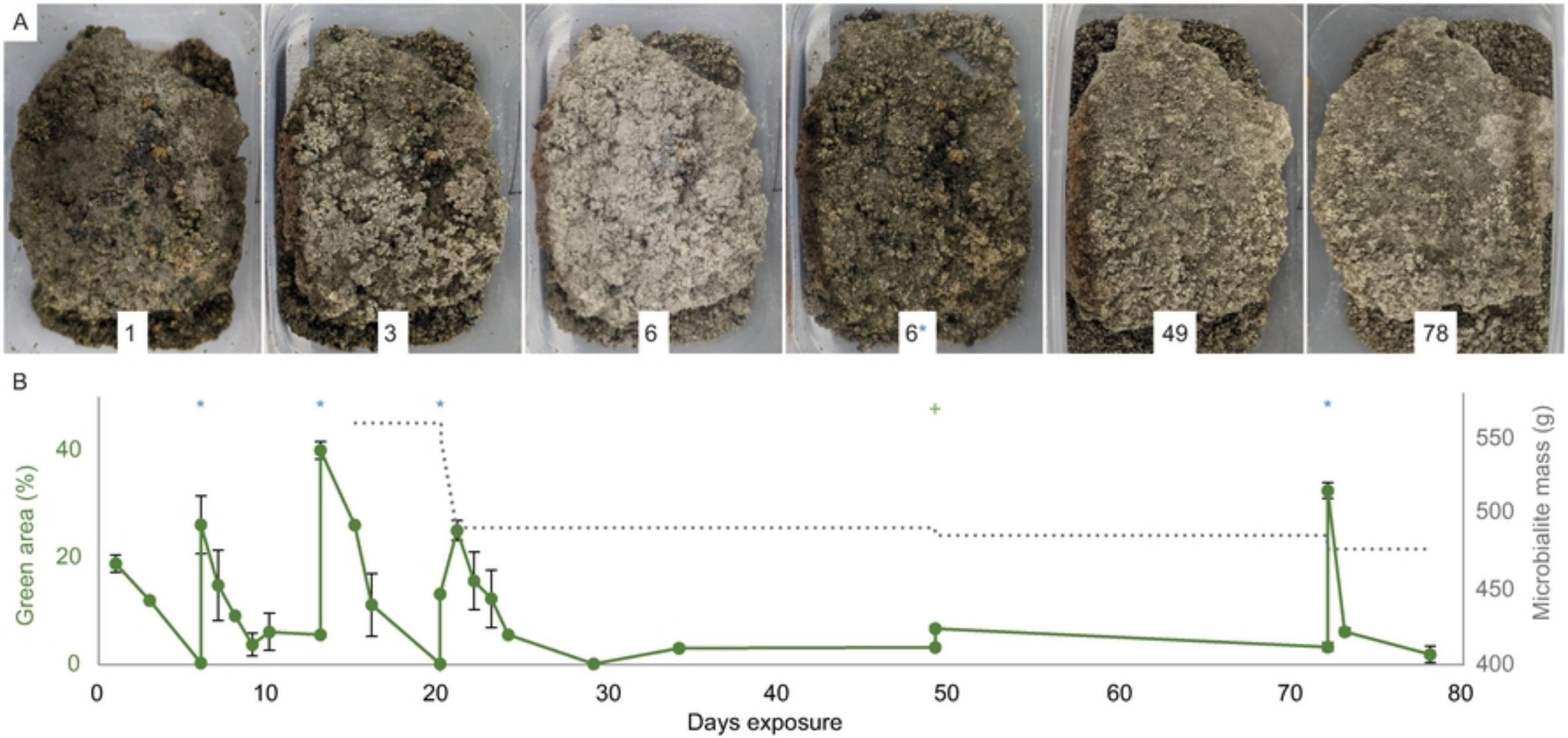

Fig 10. Lab desiccation experiment results

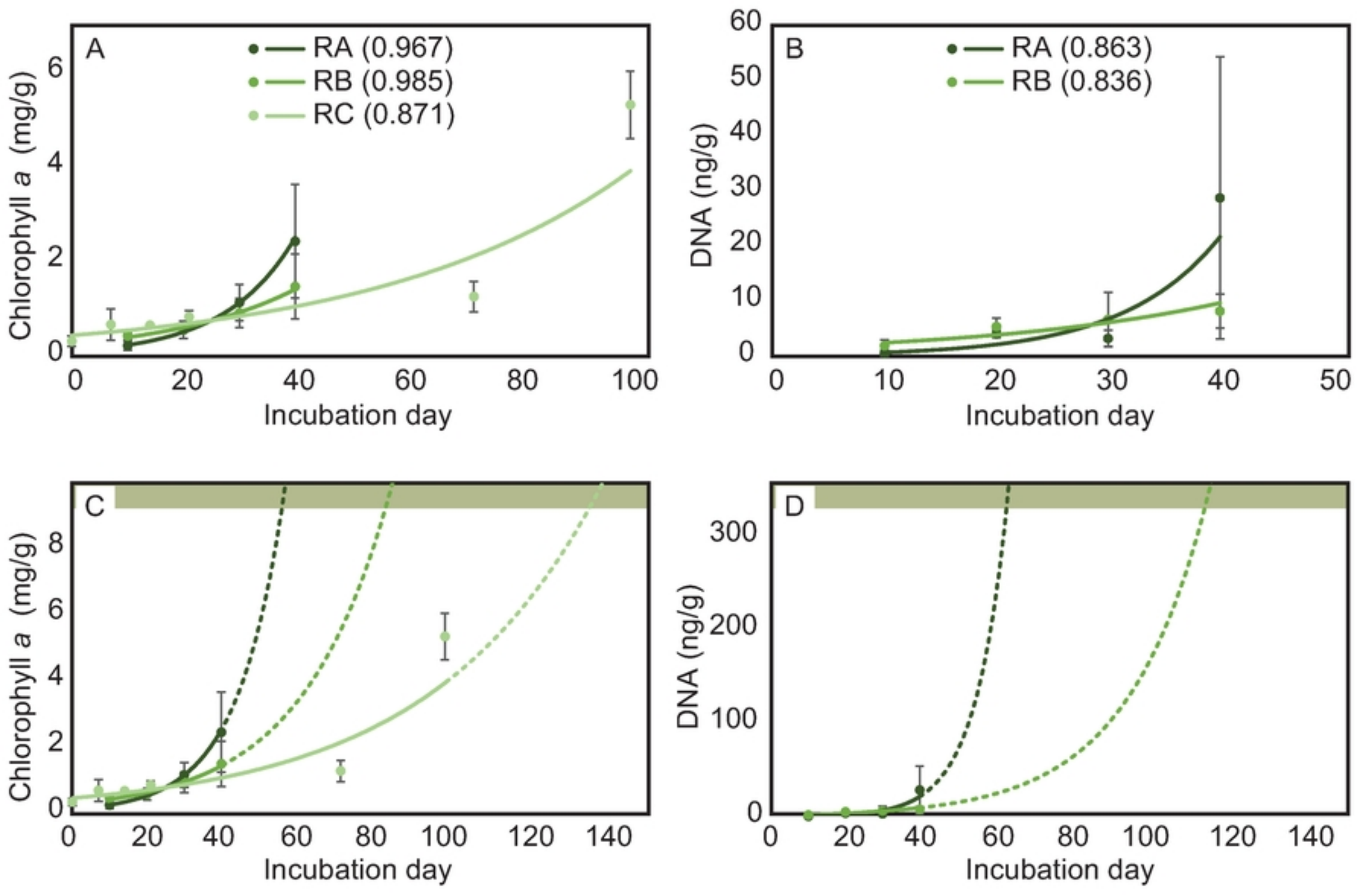

Fig 11. Recovery experiment results

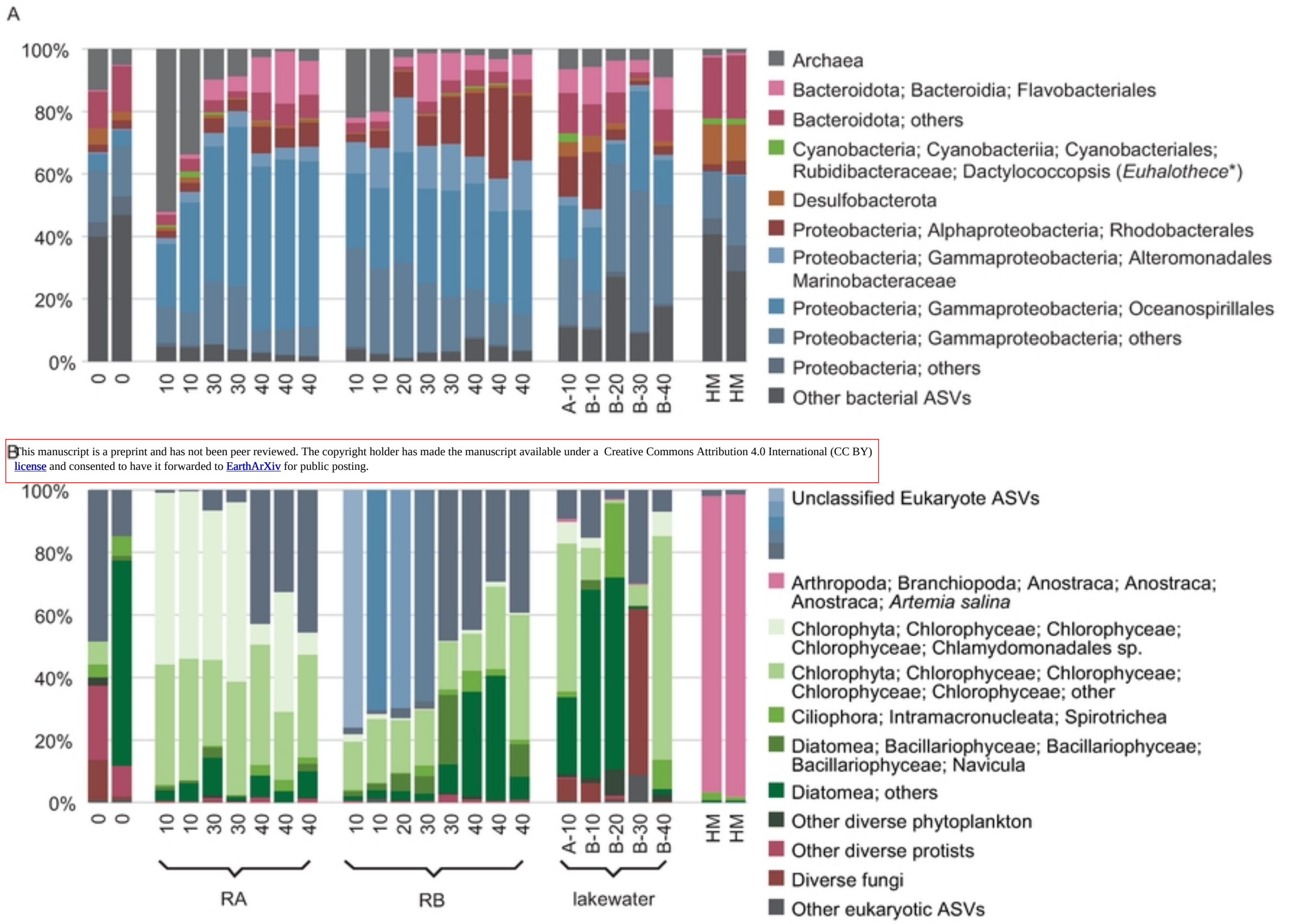

Fig 12. Recovery experiment DNA sequencing results

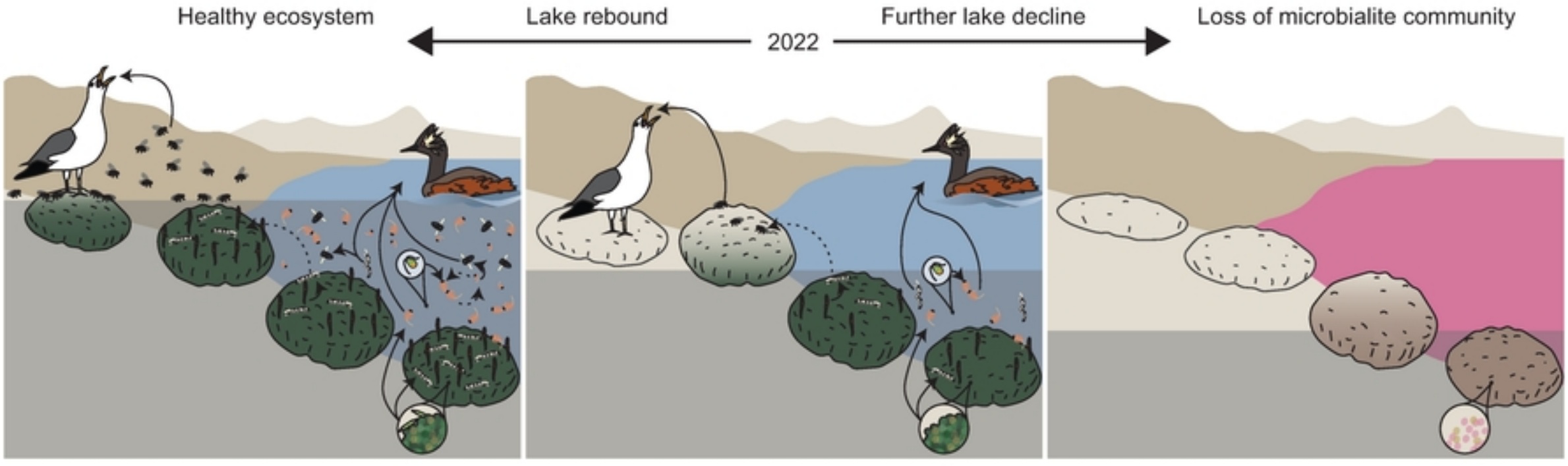

Fig 13. Summary of the big-picture findings of this study